SISSA

PAPER • OPEN ACCESS

The CMS Fast Beam Condition Monitor for HL-LHC

View the article online for updates and enhancements.

16TH TOPICAL SEMINAR ON INNOVATIVE PARTICLE AND RADIATION DETECTORS
SIENA, ITALY
25–29 SEPTEMBER 2023

The CMS Fast Beam Condition Monitor for HL-LHC

G. Auzinger [a] H. Bakhshiansohi [h] A. Dabrowski [a] A.G. Delannoy [m,*]
A. Dierlamm [i] M. Dragicevic [f] A. Gholami [h] G. Gomez [g] M. Guthoff [c]
M. Haranko [a] A. Homna [a] M. Jenihhin [o] J. Kaplon [a] O. Karacheban [k,a,*]
B. Korcsmáros [b] W.H. Liu [m,a] A. Lokhovitskiy [l] R. Loos [a] S. Mallows [i] J. Michel [a]
V. Myronenko [c] G. Pásztor [d,*] M. Pari [a] J. Schwandt [e] M. Sedghi [h] A. Shevelev [j]
K. Shibin [o] G. Steinbrueck [e] D. Stickland [j] B. Ujvari [b] and G.J. Wegrzyn [a]

[a]*CERN, European Organization for Nuclear Research, Geneva, Switzerland*

[b]*University of Debrecen, Debrecen, Hungary*

[c]*Deutsches Elektronen-Synchrotron, Hamburg, Germany*

[d]*ELTE Eötvös Loránd University, Budapest, Hungary*

[e]*University of Hamburg, Hamburg, Germany*

[f]*HEPHY, Wienna, Austria*

[g]*Instituto de Física de Cantabria (IFCA), CSIC-Universidad de Cantabria, Santander, Spain*

[h]*Isfahan University of Technology, Isfahan, Iran*

[i]*Karlsruher Institut fuer Technologie, Karlsruhe, Germany*

[j]*Princeton University, Princeton, NJ, U.S.A.*

[k]*Rutgers, The State University of New Jersey, Piscataway, NJ, U.S.A.*

[l]*University of Canterbury, Christchurch, New Zealand*

[m]*University of Oxford, Oxford, United Kingdom*

[n]*University of Tennessee, Knoxville, TN, U.S.A.*

[o]*Tallinn University of Technology, Tallinn, Estonia*

E-mail: delannoy@cern.ch, olena.karacheban@cern.ch,
gabriella.pasztor@cern.ch

ABSTRACT: The high-luminosity upgrade of the LHC brings unprecedented requirements for real-time and precision bunch-by-bunch online luminosity measurement and beam-induced background monitoring. A key component of the CMS Beam Radiation, Instrumentation and Luminosity system is a stand-alone luminometer, the Fast Beam Condition Monitor (FBCM), which is fully independent from the CMS central trigger and data acquisition services and able to operate at all times with a triggerless readout. FBCM utilizes a dedicated front-end application-specific integrated circuit (ASIC) to amplify

---

*Corresponding author.

https://doi.org/10.1088/1748-0221/19/03/C03048

the signals from CO_2-cooled silicon-pad sensors with a timing resolution of a few nanoseconds, which enables the measurement of the beam-induced background. FBCM uses a modular design with two half-disks of twelve modules at each end of CMS, with four service modules placed close to the outer edge to reduce radiation-induced aging. The electronics system design adapts several components from the CMS Tracker for power, control and read-out functionalities. The dedicated FBCM23 ASIC contains six channels and adjustable shaping time to optimize the noise with regards to sensor leakage current. Each ASIC channel outputs a single binary high-speed asynchronous signal carrying time-of-arrival and time-over-threshold information. The chip output signal is digitized, encoded, and sent via a radiation-hard gigabit transceiver and an optical link to the back-end electronics for analysis. This paper reports on the updated design of the FBCM detector and the ongoing testing program.

Contents

1 Introduction

1.1 Upgrade of the BRIL system for the HL-LHC

The high-luminosity upgrade of the Large Hadron Collider (HL-LHC) aims to increase the peak instantaneous luminosity by a factor of $\approx$ 5–7.5 with respect to its design value. This will correspond to an average rate of interactions per bunch crossing (known as *pileup*) of $\langle PU \rangle \approx$ 140–200, in comparison to a peak pileup of $\approx$60 during LHC Run 3. The *Phase-2* upgrade of the Compact Muon Solenoid (CMS) detector is designed to ensure efficient operation up to an integrated luminosity of 4000 fb^{-1}.

The Beam Radiation, Instrumentation, and Luminosity (BRIL) project of the CMS experiment is responsible for the operation of multiple detector systems. Its main deliverables include real-time and precision measurements of the luminosity, monitoring the beam timing, the beam-induced background (BIB) rate, and the beam conditions at the CMS detector to ensure safe operation of the tracker via a beam abort functionality in case of severe beam losses and, finally, monitoring and modelling the radiation environment in the experimental cavern. The strategy of the BRIL project for Phase-2 combines different elements: maintenance and upgrade of existing detectors, development of new instrumentation, and implementation of dedicated data processing to the backend of other CMS detectors for luminosity determination. The locations of the Phase-2 BRIL subsystems are shown schematically in figure 1.

1.2 Requirements for precision luminometry and the dedicated luminosity detector

The real-time monitoring of the bunch-by-bunch luminosity and BIB is required at all times when beams are circulating. Luminosity measurement is relied upon to deliver and optimize collisions at each experiment, while the monitoring of the BIB rate is needed to guarantee the safe operation of sensitive subsystems, such as the CMS tracker. BIB can be measured after a series of unfilled bunches, typically just before a train or in the abort gap, and is expected to arrive to the FBCM location 19 ns before the collision products [1]. Furthermore, special LHC operating conditions (e.g. accelerator
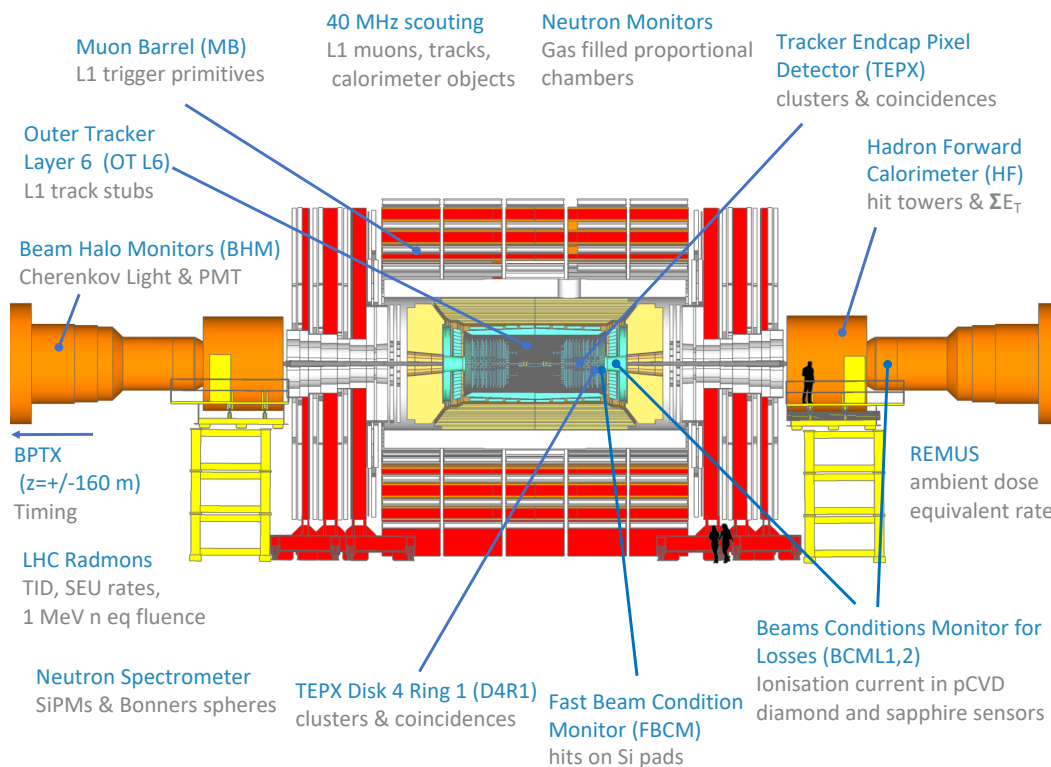
Figure 1. Subsystems of the CMS BRIL project at the HL-LHC.

commissioning and development, as well as certain periods during the machine cycle before stable beams) require the publication of online luminosity and BIB rate even when the rest of the CMS subsystems may not be in operation. In order to maximize the availability of these quantities, CMS must be equipped with a dedicated instrument which is independent in its infrastructure and operation from other CMS systems. Such a detector must be able to operate continuously regardless of the status of other subsystems, and of the central trigger and data acquisition systems. This independence also ensures flexibility to apply operational changes, such as calibrations, threshold adjustments, high-voltage adjustments, etc. for the optimal performance of the system.

An ideal luminometer is expected to show a linear response over the required dynamic range of pileup from $\langle PU \rangle \sim 0.5$ up to 200 in Phase-2. Such an instrument must report sufficient bunch-by-bunch rates to achieve sub-percent statistical precision during low-pileup running conditions that arise in special fills for absolute luminosity calibration. This is a crucial feature since luminosity detectors at hadron colliders must be independently calibrated via the van der Meer (vdM) method [2], where the effective beam overlap is measured from the detector response as a function of the transverse beam separation in special low-pileup conditions tailored to minimize beam-beam effects. An optimal luminosity detector must also offer stable long-term performance over the data-taking period, which is monitored and quantified in terms of efficiency and linearity via the analysis of short vdM-like (so-called *emittance*) scans performed during nominal pileup conditions [3].

The Fast Beam Condition Monitor (FBCM), based on silicon-pad sensors with a fast front-end chip, was proposed as a dedicated luminometer for LHC Phase-2. The detector concept was described in detail in the Phase-2 BRIL technical design report (TDR) [1]. Based on the simulations of the

detector performance, the area and the position of the sensors were optimized. The optimal location for a sensor of size 2.89 mm^2 was found to be at $r \approx 14.5$ cm. The variation in the mean number of hits per sensor per colliding bunch pair as a function of pileup based on simulation is depicted in figure 2 (left). The deviations from linearity are then shown in figure 2 (middle), featuring deviations from linearity below ±0.5%. The statistical uncertainty of the rate per second is also given in figure 2 (right), which shows that a statistical uncertainty on the rate of 0.2% is reached for the physics range of $140 < \langle PU \rangle < 200$. These simulations were done for 290 μm thick Si sensors. A new round of simulations is ongoing using the updated ASIC design [4], including the option of thinner 150 μm sensors, the alternative choice for FBCM (see in more detail in subsection 2.1).
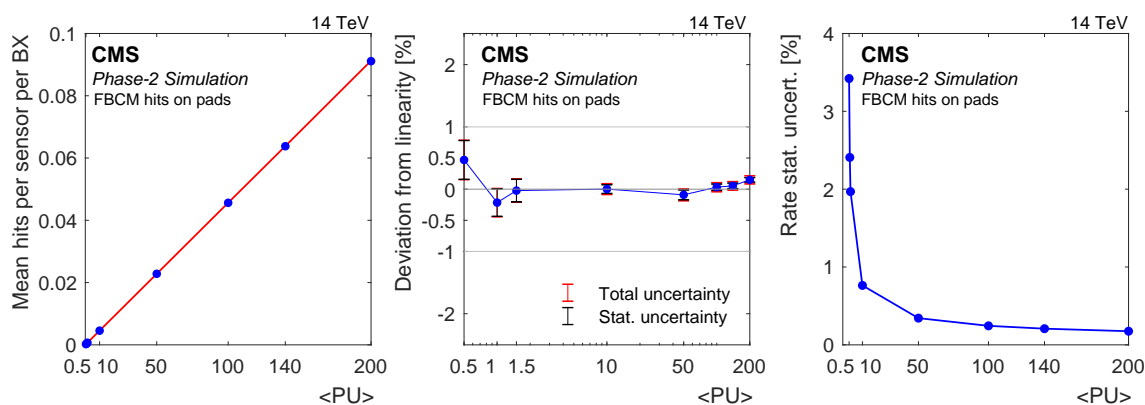

Figure 2. The mean number of hits per sensor per colliding bunch pair in the FBCM luminometer (left), the deviation of the mean hit rate from linearity (center), and the statistical uncertainty in the rate with an integration period of 1 second (right) as a function of pileup.

2 FBCM design and readout

The FBCM detector concept is based on the BCM1F detector, operated by BRIL during Run 2 and Run 3 of the LHC to provide real-time measurement of luminosity and BIB. During Run 2, BCM1F was based on a mixture of sensor technologies: in early 2017, ten silicon, ten poly-crystalline diamond (pCVD), and four single-crystal diamond (sCVD) sensors were installed [5, 6]. Since better linearity was observed for the Si-pad sensors, the sensor choice for Run 3 was changed to an all-silicon configuration with a total of 48 channels and active C_6F_{14} cooling at $-18°C$, which led to improved long-term stability and linear response [7].

The FBCM is the next generation of silicon-pad-based luminometer with symmetric and modular design, which avoids single points of failure and simplifies construction and maintenance. It features a new dedicated front-end ASIC [4], HL-LHC standard back-end electronics providing fast data processing in FPGA, and active CO_2 cooling at $-35°C$. The statistical precision is improved by installing 288 Si-pads. FBCM will be located behind the last disk of the *tracker endcap pixel* (TEPX) detector [8], close to the bulkhead, as illustrated in figure 3 (left). The cooling will be connected to the TEPX manifold.

A minimal number of connections per half-disk is foreseen to simplify the installation. Each half-disk is attached mechanically with two screws. Each has a single optical connector, and all
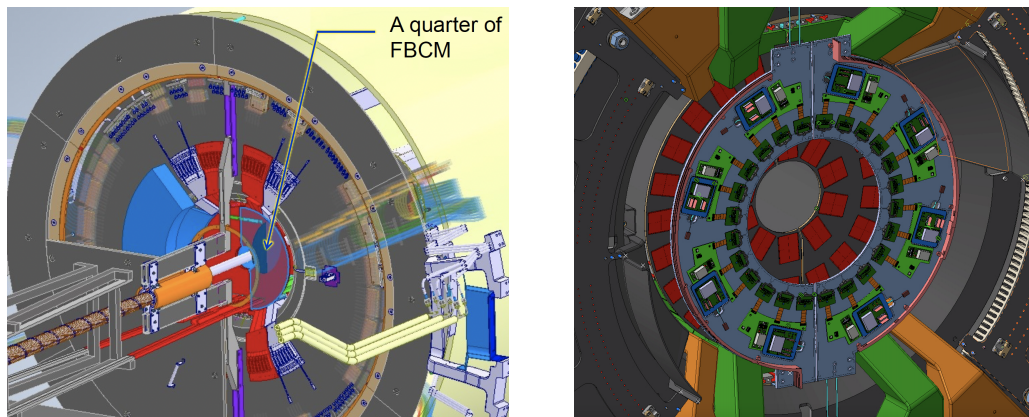
Figure 3. Sketch of the FBCM location behind the last disk of the inner tracker (left) and a zoom to the two FBCM half discs forming a ring around the beam pipe with a detailed representation of the components on each service quadrant (right).
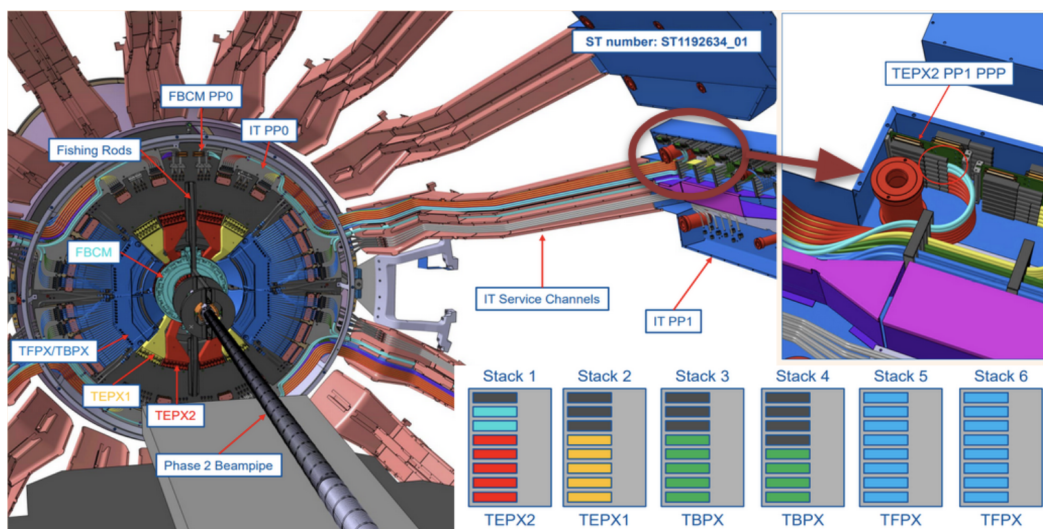

Figure 4. FBCM half-disk installation location and position of the patch panels to route the services.

power connections are provided using two multiservice cables developed for the tracker upgrade. The FBCM cables will be routed, along with TEPX cables, as shown in turquoise in figure 4 at stack 1. A custom patch panel (PP0) will be designed to route all power lines from the inner tracker patch panel (PP1) to FBCM. The powering scheme was outlined in the technical design report [1] and will be finalized in 2024 with the production of the first disk prototype. Multiple changes were introduced for the mechanical design of the detector to make space for the optical fiber routing and to optimize the thermal contacts.

The detector is segmented into four mechanically-identical and independent half-disks with inner radius of 8 cm and outer radius of 30 cm. Two half-disks form a ring around the beam pipe (figure 3 (right)) about 280 cm away from the interaction point on both ends of CMS. Each half-disk is composed of four identical *service quadrants*, as indicated in figure 5 (left). Each service quadrant has an inner tracker (IT) portcard [9], a bPol12V DC-DC converter [10] (12 V → 1.25 V), and a
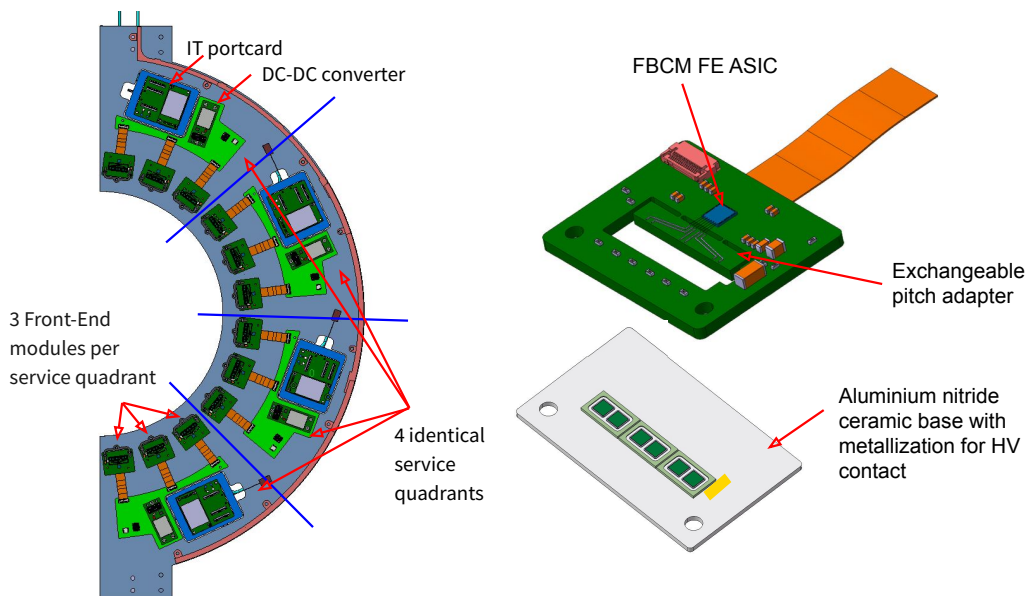
Figure 5. FBCM half-disk (left), as well as the FBCM front-end module and Aluminium-Nitride ceramic base-plate with three two-pad silicon sensors (right).

service board [8], which routes the low voltage and high voltage lines to power three front-end (FE) modules. Each FE module consists of a hybrid printed circuit board (PCB) housing the ASIC that reads out the signal from six silicon pad sensors. The 3×3 mm^2 front-end ASIC is equipped with a fast amplifier and a comparator and produces an analog pulse whose rising edge defines the *time of arrival* (ToA) and its duration, defined as the *time over threshold* (ToT), provides information on the deposited charge. The readout is triggerless. The signals are routed to the IT portcard *low-power gigabit transceiver* [11] (lpGBT) which continuously samples and transmits it to the back-end over an optical link via the *versatile link plus transceivers* [12] (VTRx+). The lpGBT sampling time interval can be as low as 0.78 ns, providing 32 samples per bunch crossing.

The FE hybrid consists of a rigid PCB with an incorporated pitch adapter matching the sensor pads to those of the ASIC, an opening for the sensors, and a flex tail which routes power connections from the service board to the FE hybrid (figure 5 (right)). Silicon sensors are attached with conductive glue to the Aluminium-Nitride (AlN) ceramic baseplate. Using alignment holes placed in the corners of the hybrid and the baseplate, the sensors are positioned in the opening of the hybrid and then bonded to the ground and, via the pitch adapter, to the ASIC channels. The surface area of the AlN plate is 30×20 mm^2 and it provides cooling contact under the sensors and via the hybrid to the ASIC. An 18 µm thick layer of copper metalization with golden finish is applied to the AlN ceramic baseplate to provide high voltage via a wire-bond from the FE board PCB to the sensor back-plane. The AlN material choice is motivated in subsection 2.2. The ASIC is wire bonded to the FE module PCB, its position on the PCB is shown in figure 5 (left). The ASIC is designed to withstand 200 MRad of total ionizing dose. The noise from the ASIC is below 900 e$^-$. The first prototype of the FBCM23 ASIC is currently mounted on a testboard that also serves as the prototype of the FE hybrid. Since its arrival in September 2023, the ASIC is undergoing extensive testing [4]. Irradiation tests, including total ionizing dose (TID) and Single Event Upset (SEU) tests, are in the pipeline.

The *Apollo* board [13] with two powerful FPGAs, developed for the ATCA crate standard, was chosen for FBCM back-end data processing. The digital processing unit in the FPGA determines the rising edge and pulse duration, and it aggregates the histograms of the number of hits per bunch crossing identification number (BCID).

2.1 Sensor design options

Two types of sensors are considered for the FBCM, shown in figure 6: a two-pad, 290 µm thick sensor which is used in the Run 3 BCM1F system and manufactured on the half-moons of the CMS Phase-2 outer tracker wafers; and a six-pad, 150 µm thick sensor printed on the half-moons of the CMS Phase-2 inner tracker wafers.

At the FBCM sensor location, the expected 1 MeV neutron equivalent fluence is about 2.5 $\times 10^{15}$ cm^{-2} for 3000 fb^{-1} (TID of 200 MRad). Due to the expected harsh radiation environment, a replacement of the FBCM is planned after about 1500 fb^{-1} (TID of 100 MRad). Beyond this fluence, the two-pad sensors are not expected to be operational with the required performance. For comparison, at the outer tracker location, the expected fluence is about 1.5×10^{15} cm^{-2}, and at the inner tracker location, about 1×10^{16} cm^{-2}. The thicker sensors have better signal-to-noise (S/N) ratio (pre-irradiation S/N = 35; after 1×10^{15} cm^{-2} irradiation S/N = 10.7), but larger leakage current. The thinner sensors are more radiation tolerant and have smaller leakage current, but have smaller signal-to-noise ratio (pre-irradiation S/N = 17; after 1.5×10^{15} cm^{-2} irradiation S/N = 8).

The single-pad size for both types of the sensors is about 1.7×1.7 mm^2. There is a difference of a few mm in the length of the six-sensors panel depending on the sensor choice. Using three two-pad sensors results in a longer panel due to sensor edges. Another significant difference arises from the guard ring structure as the new six-pad sensor features a double ring to improve its performance. The replaceable pitch adapter (see figure 6 (right)) allows both types of sensors to be used in the final assembly. Pitch adapters with several different bonding pad sizes were also produced to evaluate the effect of the parasitic capacitance from the pitch adapter on the signal. The final sensor choice will be decided in 2024 after a full set of laboratory tests and beam tests with the ASIC and both types of sensors after irradiation. Both sensor types are available in large quantity.

2.2 Thermal optimization

The longevity of FBCM system strongly depends on the efficient cooling of the sensors. Better thermal contact reduces the dark currents in the silicon sensors and, therefore, extends the lifetime of the detector before a replacement is required. This is especially important at total ionizing doses approaching 100 MRad. The FE hybrid design is thermally optimized by incorporating a 0.38 mm thick AlN ceramic baseplate with excellent thermal conductivity of about 180 W/mK, as shown in figure 5 (right). As a thermal interface between the AlN and the pocofoam (carbon foam) block, the radiation hard MORESCO RG-42R-1 grease [14] with 70% diamond powder will be used to improve thermal contact. A cooling pipe is placed at the radius of the silicon sensor's location and, on the return path, under the portcard and the bPol12V DC-DC. Pocofoam blocks (with thermal conductivity of 45 W/mK in plane and 145 W/mK out of plane) will be placed around the cooling pipe to provide thermal contact for AlN under the sensors and as a cooling pad under the bPol12V DC-DC converters.
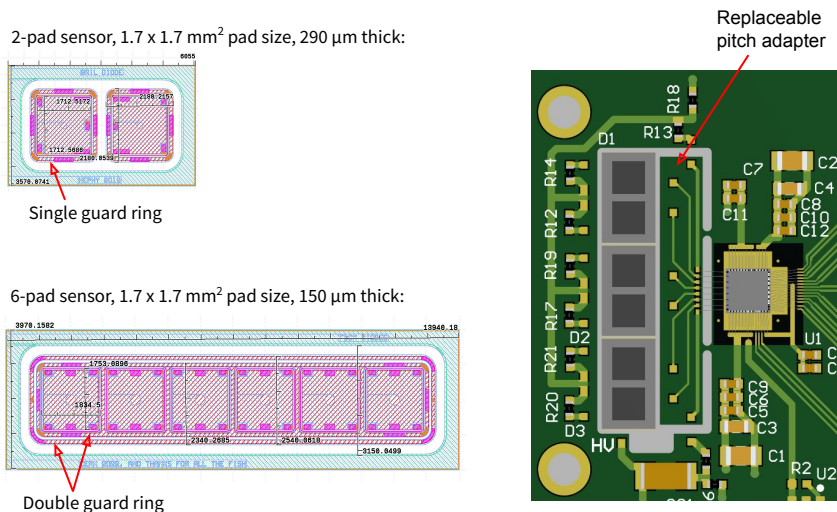
Figure 6. The two sensor designs for FBCM: a two-pad sensor used in the Run 3 BCM1F (top left), and a new six-pad sensor with double guard ring structure (bottom left), and the FE module prototype with replaceable pitch adapter (right).
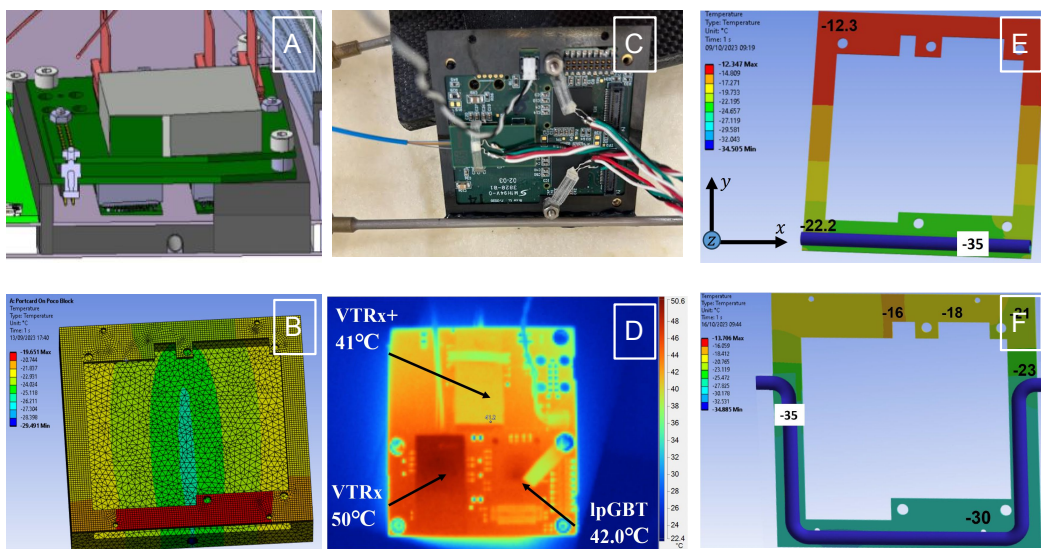

Figure 7. A portcard mounted on the FBCM half-disk with a pocofoam insert providing the thermal contact (A). Comparison of several options validated in ANSYS simulation for the connection of the cooling pipe and the carbon frame (B, E, F). The setup with portcard mounted on the cooling frame that is attached to a straight cooling pipe and thermal sensors (C). Thermal camera measurement of a powered portcard (D).

Several alternative design options were evaluated for the portcard cooling, as shown in figure 7. They include a straight cooling pipe routed through the pocofoam block and carbon frame on top of it. The drawing of this design is shown in figure 7A, and the corresponding thermal simulation in figure 7B. From the thermal simulation, it is apparent that one side of the frame is not well cooled. The simulations of the portcard cooling solutions were performed using *ANSYS Mechanical Workbench*. Another evaluated option was to attach one edge of the carbon frame directly to the cooling pipe.
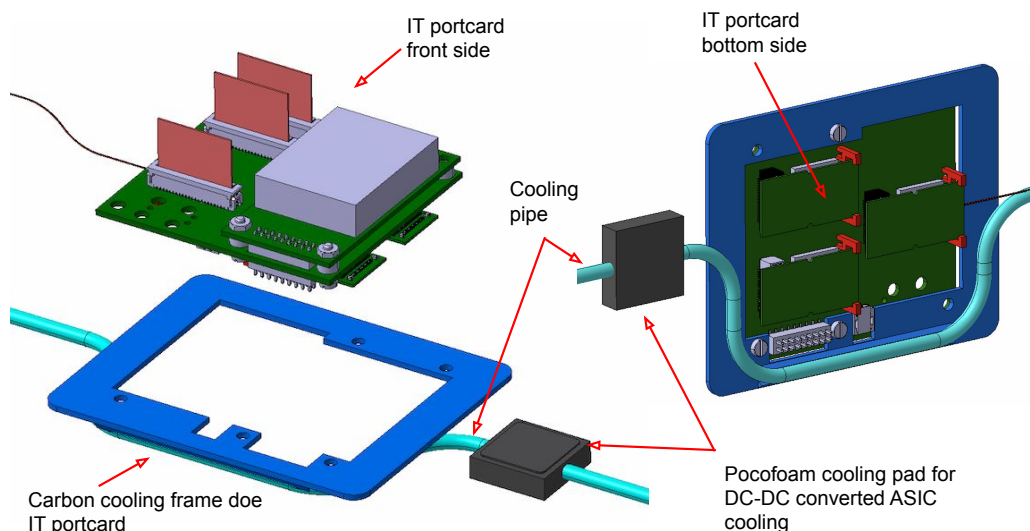
– 7 –

Figure 8. Optimized mounting of the portcard using a carbon frame directly in contact with a bent cooling pipe underneath.

The picture of the test setup is shown in figure 7C, and the thermal simulation on figure 7E. This option only provides good cooling on the contact side. Figure 7D illustrates the location of the heat sources on the portcard. Finally, a bent cooling pipe that follows half of the contour of the carbon frame, as shown in figure 7F, provides the best cooling performance.

The updated detector design with the portcard cooling frame and a bent pipe is shown from the front and back sides in figure 8. The cooling pipe is glued to the carbon frame with diamond-doped epoxy. Simulation results agree well with the measurements using PT1000 thermal sensors [15] and a thermal camera. The setup was closed in a hermetic box with a flow of dry air. Thermal camera measurements were only possible at room temperature, when the lid of the box was open. Therefore, measurements by the PT1000 thermal sensors were first compared at room temperature to the thermal camera heat map. A thermal camera measurement without cooling is shown in figure 7D, where it is visible that the VTRx+ at $50°$ C and the lpGBT at $42°$ C are the hottest components. With cooling at $-10°$ C, the temperature of all components was reduced to below $20°$ C. The cooling performance of the Phase-2 detector is foreseen to be significantly better at $-35°$ C.

3 Assembly procedure of FBCM half-disk

Figure 9 illustrates the FBCM integration process. The integration stages are shown from right to left. First, the top carbon fiber sheet is placed on a vacuum plate. Next, the pocofoam cooling pads under the sensor and DC-DC converter locations are fitted into the cut-outs and they are glued under vacuum, together with the airex foam as a spacer. Then, the groove for the cooling pipe is machined and the cooling pipe is inserted into the groove using a thin layer of thermally-conductive diamond-doped epoxy. Finally, the assembly is flattened with a vacuum bag, the bottom carbon fiber sheet is glued on top, and the carbon cooling frames for the portcards are glued on the cooling pipe.
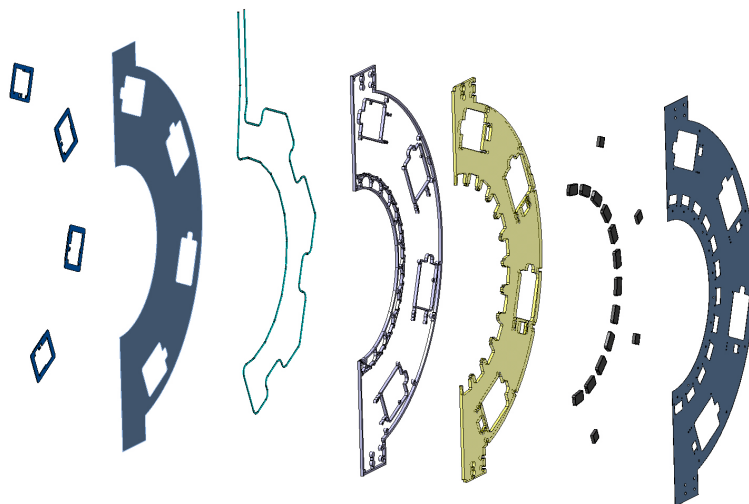
Figure 9. From right to left, the FBCM half-disk integration process step by step.

4 Summary

The Fast Beam Condition Monitor is a dedicated luminosity and beam-induced background monitor based on silicon-pad sensors with a fast front-end designed for the Phase-2 upgrade of the CMS detector. It is expected to operate continuously and independently from the central CMS data acquisition and trigger systems, and regardless of the status of other CMS subsystems. It is designed to have a linear response, from the low pileup conditions during calibration fills, up to the very large pileup values expected in HL-LHC physics conditions.

The FBCM has a symmetric and modular design to avoid single points of failure and simplify maintenance. The design of the mechanics and cooling has significantly matured since the TDR [1], with several optimizations to simplify the integration and installation, and simulation studies to deliver the best cooling performance.

Six silicon-pad sensors are read out by an ASIC, designed for the FBCM, in each front-end module. The first prototype of the ASIC is undergoing detailed tests at CERN. Two types of silicon-pad sensors are under consideration, with a trade off between the signal-to-noise ratio and leakage current. The design of the front-end modules has been thermally optimized with an Aluminium-Nitride ceramic baseplate to maximize the lifetime of the sensors.

The development and prototyping of the FBCM is on track for the Phase-2 CMS upgrade for HL-LHC. FBCM will be instrumental for achieving the target precision in luminosity measurement (2% online; <1% offline) during the HL-LHC era.

References

[1] C.M.S. Collaboration, *The Phase-2 Upgrade of the CMS Beam Radiation Instrumentation and Luminosity Detectors*, CERN-LHCC-2021-008, CERN, Geneva (2021).

[2] CMS collaboration, *Precision luminosity measurement in proton-proton collisions at $\sqrt{s}$ = 13 TeV in 2015 and 2016 at CMS*, *Eur. Phys. J. C* **81** (2021) 800 [arXiv:2104.01927].

[3] O. Karacheban and P. Tsrunchev, *Emittance scans for CMS luminosity calibration*, *EPJ Web Conf.* **201** (2019) 04001.

[4] J. Kaplon, G. Wegrzyn, K. Shibin and M. Barendregt, *The optimization, design and performance of the FBCM23 ASIC for the upgraded CMS beam monitoring system*, 2024 *JINST* **19** C02026 [arXiv:2312.02834].

[5] A.A. Zagozdzinska et al., *New Fast Beam Conditions Monitoring (BCM1F) system for CMS*, 2016 *JINST* **11** C01088.

[6] M. Guthoff, *The new Fast Beam Condition Monitor using poly-crystalline diamond sensors for luminosity measurement at CMS*, *Nucl. Instrum. Meth. A* **936** (2019) 717.

[7] J. Wańczyk, *Upgraded CMS Fast Beam Condition Monitor for LHC Run 3 Online Luminosity and Beam Induced Background Measurements*, *JACoW I* **BIC2022** (2022) 540.

[8] CMS collaboration, *The Phase-2 Upgrade of the CMS Tracker*, CERN-LHCC-2017-009, CERN, Geneva (2017) [DOI:10.17181/CERN.QZ28.FLHW].

[9] S. Orfanelli, *The CMS Inner Tracker electronics system development*, 2022 *JINST* **17** C08003.

[10] F. Faccio et al., *The bPOL12V DCDC converter for HL-LHC trackers: towards production readiness*, *PoS* **370** (2020) 070.

[11] S. Biereigel et al., *The lpGBT PLL and CDR Architecture, Performance and SEE Robustness*, *PoS* **TWEPP2019** (2020) 034.

[12] C. Soós et al., *Versatile Link PLUS transceiver development*, 2017 *JINST* **12** C03068.

[13] A. Albert et al., *The Apollo ATCA Platform*, *PoS* **TWEPP2019** (2020) 120 [arXiv:1911.06452].

[14] M. Ferrari et al., *Selection of radiation tolerant commercial greases for high-radiation areas at CERN: Methodology and applications*, *Nucl. Mater. Energy* **29** (2021) 101088.

[15] V.M. Miklyaev, Y.P. Filippov and A.Y. Filippov, *Application of Pt1000 C420 Thin-Film Temperature Sensors at Superconducting and Other Types of Facilities*, *Phys. Part. Nucl. Lett.* **17** (2020) 44.